Global heat stress on health, wildfires, and agricultural crops under different levels of climate warming

Qiaohong Sun, Chiyuan Miao, Martin Hanel, Alistair G. L. Borthwick, Qingyun Duan, Duoying Ji, & Hu Li

2019

Pacific Climate Impacts Consortium (PCIC)

PCIC Publications

Original citation:

Sun, Q., Miao, C., Hanel, M., Borthwick, A. G. L., Duan, Q., Ji, D., & Li, H. (2019). Global heat stress on health, wildfires, and agricultural crops under different levels of climate warming. *Environment International*, *128*, 125–136. https://doi.org/10.1016/j.envint.2019.04.025

Environment International 128 (2019) 125–136

Contents lists available at ScienceDirect

Environment International

journal homepage: www.elsevier.com/locate/envint

Global heat stress on health, wildfires, and agricultural crops under different levels of climate warming

Qiaohong Sun[a], Chiyuan Miao[a,*], Martin Hanel[b], Alistair G.L. Borthwick[c], Qingyun Duan[a], Duoying Ji[d], Hu Li[e]

[a] State Key Laboratory of Earth Surface Processes and Resource Ecology, Faculty of Geographical Science, Beijing Normal University, Beijing 100875, China
[b] Faculty of Environmental Sciences, Czech University of Life Sciences, Prague 16900, Czech Republic
[c] School of Engineering, University of Edinburgh, The King's Buildings, Edinburgh EH9 3JL, UK
[d] College of Global Change and Earth System Science, Beijing Normal University, Beijing 100875, China
[e] Key Laboratory of Agricultural Non-point Source Pollution Control, Ministry of Agriculture/Institute of Agricultural Resources and Regional Planning, Chinese Academy of Agricultural Sciences, Beijing 100081, China

ARTICLE INFO

Handling Editor: Hanna Boogaard

Keywords:
Global warming
Exposure
Heat-related extremes
1.5 °C warming target

ABSTRACT

The effects of heat stress are spatially heterogeneous owing to local variations in climate response, population density, and social conditions. Using global climate and impact models from the Inter-Sectoral Impact Model Intercomparison Project, our analysis shows that the frequency and intensity of heat events increase, especially in tropical regions (geographic perspective) and developing countries (national perspective), even with global warming held to the 1.5 °C target. An additional 0.5 °C increase to the 2 °C warming target leads to > 15% of global land area becoming exposed to levels of heat stress that affect human health; almost all countries in Europe will be subject to increased fire danger, with the duration of the fire season lasting 3.3 days longer; 106 countries are projected to experience an increase in the wheat production-damage index. Globally, about 38%, 50%, 46%, 36%, and 48% of the increases in exposure to health threats, wildfire, crop heat stress for soybeans, wheat, and maize could be avoided by constraining global warming to 1.5 °C rather than 2 °C. With high emissions, these impacts will continue to intensify over time, extending to almost all countries by the end of the 21st century: > 95% of countries will face exposure to health-related heat stress, with India and Brazil ranked highest for integrated heat-stress exposure. The magnitude of the changes in fire season length and wildfire frequency are projected to increase substantially over 74% global land, with particularly strong effects in the United States, Canada, Brazil, China, Australia, and Russia. Our study should help facilitate climate policies that account for international variations in the heat-related threats posed by climate change.

1. Introduction

The Paris Agreement has responded to the risks from climate change by setting a global collective goal "to hold warming well below 2 degrees, with efforts to limit warming to 1.5 degrees" above pre-industrial averages. Wide ranging, sound scientific analysis of the impact of different levels of warming on the local climate in different regions is crucial for multi-level decision-making processes. Recently, several studies have quantitatively analyzed the risks and impacts of different levels of warming on different sectors (AghaKouchak et al., 2014; Baker et al., 2018; Cai et al., 2018; Kharin et al., 2018; King and Harrington, 2018; King et al., 2017; Schleussner et al., 2016). For instance, dryland areas are the most sensitive and vulnerable to global warming, with ~44% more warming likely to occur in dry regions than in humid regions under 2.0 °C global warming, and increased risks of adverse agricultural, hydrological, drought-related, and health-related impacts in drylands if global warming were to rise from 1.5 °C to 2.0 °C (Huang et al., 2017). Drought risk increases more significantly in Mediterranean areas and central Europe than in the southwest and Central Great Plains regions of the U.S. for both 1.5 °C and 2.0 °C warming targets, with the additional 0.5 °C leading to substantially higher risk (Lehner et al., 2017). In terms of extreme precipitation, Zhang et al. (2018) reported that 0.5 °C less warming (i.e. 1.5 °C versus 2.0 °C) could lead to an 18–41% reduction in changes in areal exposures to dangerous extreme precipitation events, and a 36% (22–46%) reduction in changes in population exposure. To preserve > 10% of the coral reefs worldwide, it is believed that the global mean temperature change must be kept below 1.5 °C; under global warming of > 2.0 °C, coral reefs will no

* Corresponding author at: Faculty of Geographical Science, Beijing Normal University, Beijing 100875, China.
E-mail address: miaocy@vip.sina.com (C. Miao).

https://doi.org/10.1016/j.envint.2019.04.025
Received 25 November 2018; Received in revised form 22 March 2019; Accepted 9 April 2019
Available online 03 May 2019

longer form a prominent part of coastal ecosystems (Frieler et al., 2013; Jia and Gao, 2017). Many previous studies have made great efforts to understand the different climatic impacts of the two warming levels at regional scale. In Australia (King et al., 2017), Europe (King and Karoly, 2017), the Middle East, Africa (Ahmadalipour and Moradkhani, 2018; Nangombe et al., 2018), and East Asia (Li et al., 2018a, 2018b; Zhou et al., 2018, 2018a; Wang et al., 2017), the likelihood of experiencing record-breaking, high-impact extreme climate events is predicted to increase considerably with 1.5 °C and 2.0 °C increases in the global mean temperature.

Higher average temperatures generally result in increased heat stress (AghaKouchak et al., 2015; Fischer and Knutti, 2015; Sun et al., 2017; Ahmadalipour and Demirel, 2017). Constraining global warming to 1.5 °C, rather than 2 °C, would benefit many regions (Russo et al., 2019; Zhou et al., 2018; Wang et al., 2017; Xu et al., 2017; Gao et al., 2019). In Africa, stabilizing global warming below 1.5 °C would lead to a one-fifth reduction in the occurrence of extreme high-temperature events (Nangombe et al., 2018). In East Asia, 35%–46% of the increases in extreme high-temperature events could be avoided if global warming is kept beneath 1.5 °C (Li et al., 2018a, 2018b). In China, > 6% of the increase in summer days and 11% of the increase in tropical nights could be avoided, particularly in north China (Li et al., 2018a, 2018b). The risk of heatwaves and the exposure to heatwaves could be significantly reduced in both developing and highly developed countries if warming is limited to 1.5 °C instead of 2 °C (Russo et al., 2019). However, most of these previous studies focused mainly on changes in heatwaves and other high-temperature events. High heat stress occurring simultaneously with other extreme weather conditions leads to severe consequences for a range of sectors, exacerbating risks to human health and economic productivity. For instance, extremely high temperatures in combination with high relative humidity raise human morbidity and mortality rates (Fischer and Schar, 2010; Matthews et al., 2017). Concurrence of heatwaves and drought increases the risk of wildfires (Williams et al., 2013). Extreme heat stress during the crop reproductive period is detrimental to crop productivity (Deryng et al., 2014; Teixeira et al., 2013; Yang et al., 2019). Analysis of the change in the impact of heat stress on multiple sectors under 1.5 °C and 2.0 °C warming scenarios is necessary to enable more precise risk assessments. Furthermore, the effects of heat stress are likely to exhibit regional variations within a country, owing to spatial heterogeneity of the climate response, non-uniform population density, and variations in social conditions. Heavily populated regions are particularly susceptible to the threat posed to human well-being by extreme heat events (Diffenbaugh et al., 2007). Quantification of the potential spatial heterogeneity in climate-related exposure to heat stress at the country level is required to identify where and to what extent lives and livelihoods will be at risk in the future, and to facilitate more reasonable mitigation of international climate change.

Therefore, our study aims to provide a spatially explicit assessment of changes in heat stress across multiple sectors under 1.5 °C and 2.0 °C global warmings, using global climate and impact models from the Inter-Sectoral Impact Model Intercomparison Project (ISI-MIP), and identify national variations in climate-related exposure by combining hazard impacts with non-climate factors.

2. Materials and methods

2.1. Climate models

In this study, we assessed the impact of the 1.5 °C and 2.0 °C warming targets on three sectors: health, agriculture, and wildfires. Climate datasets were based on projections drawn from the ISI-MIP Fast Track database. Climate simulations were drawn from five global climate models: GFDL-ESM2M, HadGEM2-ES, IPSLCM5A-LR, MIROC-ESM-CHEM, and NorESM1-M. The data from these five models are bilinearly interpolated into a 0.5° × 0.5° spatial grid, and the models cover temporal ranges from 1981 to 2005 (historical simulations) and 2006 to 2099 [future projections under Representative Concentration Pathway (RCP) 8.5] (Hempel et al., 2013). There are several reasons why we selected these five ISI-MIP models. First, the climate model data are corrected using a trend-preserving statistical bias-correction method, which adjusts the monthly mean and daily variability of the simulated climate data to the observations to ensure long-term statistical agreement with the observation-based forcing data. By comparing global maps of different statistical quantities of uncorrected and bias-corrected GCM data for the period from 1980 to 1999, Hempel et al. (2013) demonstrated that this approach performs well when adjusting the probability distribution over the reference period. Second, the climate sensitivities of the climate models are retained, and the projected trends in all other variables are preserved (Hempel et al., 2013). Lastly, the ISI-MIP data have been used for many impact projections (Rosenzweig et al., 2014) at different projected levels of global warming.

Table 1
ISI-MIP models used in the projections, with respective 20-year time slices for 1.5 °C and 2.0 °C warmings.

Model	1.5 °C	2.0 °C
GFDL-ESM2M	2028, 2047	2044, 2063
HadGEM2-ES	2010, 2029	2022, 2041
IPSL-CM5A-LR	2016, 2035	2029, 2048
MIROC-ESM-CHEM	2010, 2029	2022, 2041
NorESM1-M	2022, 2041	2038, 2057

We used 20-year time slices for 1.5 °C and 2.0 °C global warmings identified for the RCP 8.5 scenario by Schleussner et al. (2016). Time slices for the individual GCMs are given in Table 1. The timings of the 1.5 °C and 2 °C warming scenarios above pre-industrial levels are determined using the 20-year running average global mean surface air temperature separately for each model. Warming levels are derived relative to the reference period 1986–2005 [this reference period is 0.6 °C warmer than pre-industrial levels (1850–1900)], and translate to warmings of 0.9 °C and 1.4 °C above reference period levels for the 1.5 °C and 2 °C limits, respectively. The 1.5 °C and 2 °C warming periods are then aggregated from 20-year windows centered on years when the 20-year running mean exceeded the respective warming levels. In addition to the time slices for 1.5 °C and 2.0 °C global warmings, we also assessed the changes in extreme events at the end of the 21st century (2080–2099). For each sector, we estimated the related changes and impacts derived from the simple arithmetic ensemble mean of the five models. We used Student's *t*-test to assess the significance of the changes at the 1.5 °C and 2 °C warming levels.

2.2. Health sector

Apparent temperature represents heat stress on the human body by accounting for the effects of environmental factors in addition to temperature, such as humidity, and by representing the nonlinear nature of heat stress. We used the health heat index (HHI) as a measure of apparent temperature (AT). This index is calculated from daily temperature and relative humidity (RH) values obtained from the five climate models in the ISI-MIP datasets. Computation of HHI involves a refinement of the multiple regression analysis carried out by Rothfusz (1990), as follows:

$$HHI = c_1 + c_2 \times T + c_3 \times T^2 + RH \times (c_4 + c_5 \times T + c_6 \times T^2) + RH^2 \times (c_7 + c_8 \times T + c_9 \times T^2) \quad (1)$$

where $c_1 = -42.379$, $c_2 = 2.04901523$, $c_3 = -6.83783 \times 10^{-3}$, $c_4 = 10.14333127$, $c_5 = -0.22475541$, $c_6 = 1.22874 \times 10^{-3}$, $c_7 = -0.05481717$, $c_8 = 8.5282 \times 10^{-4}$, $c_9 = -1.99 \times 10^{-6}$; T is

temperature in degrees Fahrenheit, and RH is a percentage. However, if RH > 13% and T is between 80 °F and 112 °F, then HHI is adjusted by subtracting the following value:

$$\text{Adjustment} = [(13 - \text{RH})/4] \times \sqrt{(17 - |\text{T} - 95|)/17} \quad (2)$$

If RH > 85% and T is between 80 °F and 87 °F, the following value is added to HHI:

$$\text{Adjustment} = [(\text{RH} - 85)/10] \times [(87 - \text{T})/5] \quad (3)$$

If HHI < 80 °F, then HHI is recalculated as follows:

$$\text{HHI} = 0.5 \times [\text{T} + 61 + (\text{T} - 68) \times 1.2 + 0.094 \times \text{RH}] \quad (4)$$

Details of the HHI calculation are given on the website of the National Weather Service - Weather Prediction Center (http://www.wpc.ncep.noaa.gov/html/heatindex_equation.shtml). In our study, we calculated the total number of days with an HHI > 105 °F (equivalent to 40.6 °C, hereafter referred to as AT105F). Above this threshold, heat conditions become dangerous or extremely dangerous for at-risk groups (https://www.weather.gov/safety/heat-index) and heat disorders such as heat stroke and heat exhaustion become likely (NOAA, 1985; Fischer and Schar, 2010). AT105F is the threshold at which the United States National Weather Service issues heat advisories, (https://www.weather.gov/dmx/dssheat). We used the threshold of AT105F for the entire land area.

2.3. Ecological sector

We used the McArthur Forest Fire Danger Index (FFDI) (Noble et al., 1980) to measure the degree of wildfire danger. The FFDI was calculated from the mean temperature, maximum temperature, precipitation, relative humidity, and wind data. FFDI is computed as follows:

$$\text{FFDI} = 2.0 \times e^{(-0.450 + 0.987 \ln \text{DF} - 0.0345\text{RH} + 0.0338\text{T} + 0.0234\text{U})} \quad (5)$$

where RH is the relative humidity (%), T is the surface air temperature (°C), U is the wind speed (km/h), and DF is the drought factor. The drought factor is based on the soil moisture deficit derived from the Keech-Byram drought index (KBDI, Keetch and Byram, 1968):

$$\text{DF} = 0.191 \times (\text{K} + 104) \times (\text{N} + 1)^{1.5}/[3.52 \times (\text{N} + 1)^{1.5} + \text{P} - 1] \quad (6)$$

in which N is time since rain (days), P is amount of precipitation (mm). K is the KBDI, calculated as:

$$\text{KBDI}_t = \text{KBDI}_{t-1} + \frac{[203.2 - (\text{KBDI}_{(t-1)} - \text{P}_t)] \times [0.968e^{(0.0875\text{T} + 1.5552) - 8.30)}]}{(1 + 10.88e^{-0.001736\text{P}_a})} \times 10^{-3} \quad (7)$$

where t is the time interval of 1 day, P_t is the precipitation for day t (mm), and P_a is the mean annual precipitation (mm). Then, daily FFDI values were normalized in each grid cell as described by Jolly et al. (2015):

$$\text{FFDI}_{\text{Norm}_{ij}} = \frac{\text{FFDI}_{ij} - \text{FFDI}_{\text{Min}}}{\text{FFDI}_{\text{Max}} - \text{FFDI}_{\text{Min}}} * 100 \quad (8)$$

where $\text{FFDI}_{\text{Norm}_{ij}}$ is the normalized daily FFDI, which ranges from 0 to 100, FFDI_{ij} is the daily FFDI for a given grid for day i of year j, and FFDI_{Min} and FFDI_{Max} are the historical daily minimum and maximum FFDI for the grid. Fire season length was defined as the number of days when the normalized daily fire danger index was above a threshold value of 50, following Jolly et al. (2015). We determined fire frequency using a simulation from the Vegetation Integrative SImulator for Trace Gases (VISIT), a model for simulating atmosphere–ecosystem biogeochemical interactions. We assessed changes in fire season length and fire frequency over different terrestrial ecoregions of the world. A map of terrestrial ecoregions, from Terrestrial Ecoregions of the World (TEOW) (Olson et al., 2001), was used to represent the biogeographic regionalization of the Earth's terrestrial biodiversity, which includes 867 terrestrial ecoregions classified into 14 different biomes such as forests, grasslands, or deserts (Fig. S1).

2.4. Agricultural sector

Crops are sensitive to heat stress during the reproductive phase, termed the thermal-sensitive period (TSP) which depends on species and cultivar. We defined the thermal-sensitive period as the period from anthesis to maturity, using dates estimated from a global crop model, PEGASUS provided by ISIMIP (Rosenzweig et al., 2014). When daily effective temperature (T_{eff}) exceeds a critical temperature threshold (T_{cr}), damage to crop yields may occur; maximum impact occurs if T_{eff} exceeds the limit temperature threshold (T_{lim}). We calculated the daily anthesis heat stress (AHSd) during the reproductive phase as follows:

$$\text{AHSd}_{ij} = \begin{cases} 0 & \text{if } \text{T}_{\text{eff}} < \text{T}_{\text{cr}} \\ \dfrac{\text{T}_{\text{eff}} - \text{T}_{\text{cr}}}{\text{T}_{\text{lim}} - \text{T}_{\text{cr}}} & \text{if } \text{T}_{\text{cr}} \le \text{T}_{\text{eff}} < \text{T}_{\text{lim}} \\ 1 & \text{if } \text{T}_{\text{eff}} \ge \text{T}_{\text{lim}} \end{cases} \quad (9)$$

where $T_{eff_{ij}}$ is defined as the mean of the daily mean and maximum temperatures for a given grid cell on day i during the reproductive phase of year j. T_{cr} and T_{lim} for each crop were adapted from Teixeira et al. (2013), as described in Table 2. AHSd during the thermal-sensitive period was accumulated and averaged to calculate the anthesis heat stress (AHS) from

$$\text{AHS}_j = \frac{\sum_{t=1}^{L_{TSP_j}} (\text{AHSd})}{L_{TSP_j}} \quad (10)$$

The value of AHS reflects heat stress events experienced during the thermal-sensitive period of crop growth. L_{TSP_j} is the length of the thermal-sensitive period in year j, and t (1, 2, 3, …, l) is the number of days in the thermal-sensitive period. The AHS was categorized as: very low (AHS = 0.0), low (AHS < 0.05); medium (0.05 ≤ AHS < 0.15); high (0.15 ≤ AHS ≤ 0.30); and very high (AHS > 0.30) stress intensity. We calculated the AHS for soybean, maize, and wheat over their corresponding suitable areas, identified according to the Global Harvested Area and Yield for 175 Crops dataset (Monfreda et al., 2008). Grid cells within harvested areas were defined as suitable areas for the corresponding crops (Fig. S2). We then calculated the normalized agricultural production damage index (NPDI) to estimate the magnitude of agricultural produce losses caused by heat stress. The production damage index for year j (PDI_j) at each grid cell was calculated as a product of attainable production P_{att} (crop yield times harvested area) and AHS_j. The PDI_j was then aggregated over each country and normalized by the maximum country-aggregated PDI_j during the 1981–2099 period, yielding the normalized agricultural production damage index ($NPDI_j$).

2.5. Exposure

For each sector, we constructed a country-level socio-climatic exposure index to estimate the level of threat faced by different countries from interactions between the regional climatic changes and relevant socio-economic factors. We consider integrated exposure to health-

Table 2
Parameters used to calculate anthesis heat stress.

Crop	T_{cr} (°C)	T_{lim} (°C)
Maize	35	45
Soybean	35	40
Wheat	27	40

Table 3
Input data used to construct indicators for health heat stress, wildfire risk, and crop heat stress.

Indicator	Component	Description
HHI integrated exposure	Health heat index (HHI)	Number of days with HHI > 40.6°C
	HHI area exposure	Total area with HHI > 40.6°C
	HHI population exposure	Population density within areas experiencing HHI > 40.6°C
Integrated exposure to wildfire	Fire frequency	Number of days with fire events
	Fire area exposure	Total area with fire events
	Fire season length	The number of days when the normalized daily fire danger index was above a threshold value of 50.
Integrated exposure to crop-heat stress	Anthesis heat stress (AHS)	High-temperature event occurs when the daily effective temperature (T_{eff}) exceeds a critical temperature (T_{cr}) threshold within the crop reproductive period
	Area under risk of AHS	Percentage of harvested area with AHS > 0.05

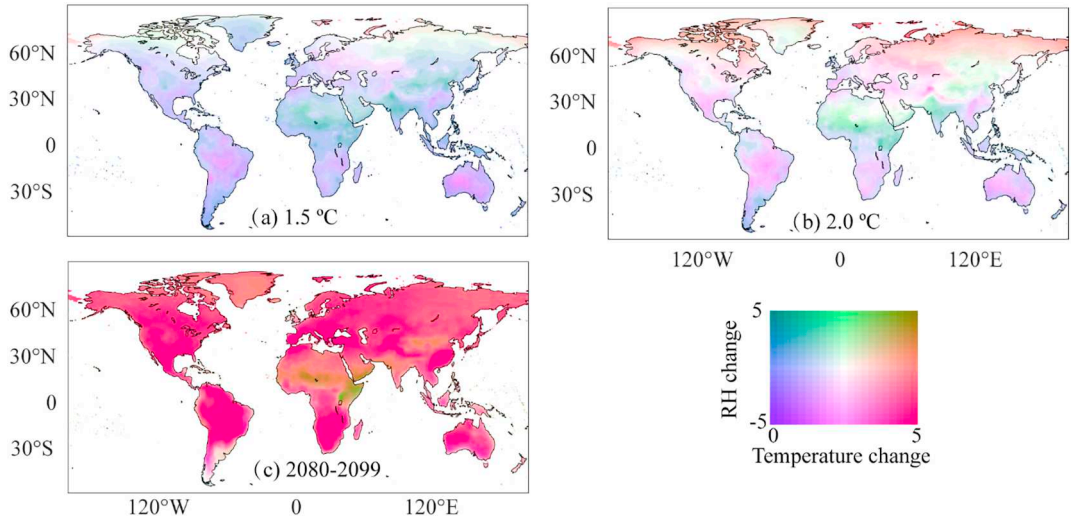

Fig. 1. Average changes in temperature and relative humidity (RH) relative to the baseline period (1981–2000). Average changes for (a) 1.5 °C and (b) 2.0 °C global warming time slices; and (c) the 2080–2099 period (RCP 8.5 scenario).

related heat stress, wild fire, and crop-related heat stress (Table 3). Exposure to events was estimated following well-established procedures described by Lung et al. (2013). First, for each 20-year time window, the individual input climatic and socio-economic indicators of exposure (defined in Table 3) were transformed into a dimensionless unit by dividing by the maximum values obtained for each indicator during the baseline period (1981–2000). Then, the dimensionless values were combined into a standardized, composite (impact) indicator via geometric aggregation (i.e. the product of weighted indicators) to achieve the following integrated exposure index (IEI):

$$IEI = \left(\prod_{i=1}^{n} I_i^{Wi}\right)^{\frac{1}{n}} \quad (11)$$

where $\{I_1, I_2, \ldots, I_n\}$ are the normalized individual input indicators. During the aggregation procedure, w is the weight for each individual input indicator; in this study, the individual indicators were given equal weight.

Populations exposed to extreme events were calculated from the "Global dataset of gridded population scenarios" (Murakami and Yamagata, 2016). We used population data from "The marker quantification of the Shared Socioeconomic Pathway 2: A middle-of-the-road scenario for the 21st century." Population data for the 2000s, 2020s, 2030s, and 2090s (Fig. S3) were used to estimate population exposure during the baseline period (1981–2000), with 1.5 °C and 2.0 °C global warming targets, and at the end of 21st century. The analysis here focuses on the SSP2 middle-of-the-road scenario (Fricko et al., 2017), which predicsts a global population of nine billion by 2100.

2.6. Avoided impacts

The proportion of impacts avoided with warming of 1.5 °C compared with warming of 2.0 °C was quantified using the function defined by Li et al. (2018a):

$$AI = \frac{E_{2.0} - E_{1.5}}{E_{2.0}} \times 100\% \quad (12)$$

where AI is the avoided impacts for exposure to different heat-related indictors. $E_{1.5}$ and $E_{2.0}$ are the changes in the 1.5 °C and 2 °C warming climate compared with the baseline period (1981–2000).

3. Results

3.1. Changes in health heat stress

Extreme high temperature is one of the greatest global natural hazards to human health. The risk of human illness and mortality increases on hot days, compounded by attendant increases in humidity, which restricts people's ability to dissipate heat. Many organizations use the health heat index (HHI) to represent apparent temperature and thus identify episodes of extreme heat. According to a chart from the United States National Weather Service that indicates the risk of heat disorders at different heat-index values, days with HHI > 105 °F (AT105F) are dangerous or extremely dangerous for at-risk groups (https://www.weather.gov/safety/heat-index). In tropical regions, including large parts of India, Africa, and northern South America, the projected simultaneous increases in daily temperature and relative humidity promote more frequent occurrences of dangerous heat levels

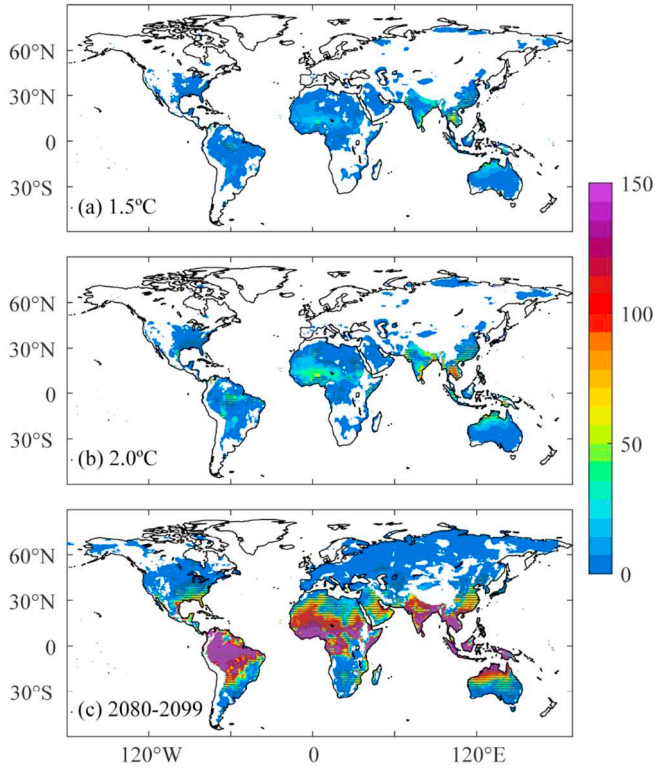

Fig. 2. Changes in number of days with HHI > 40.6 °C (105 °F) relative to the baseline period (1981–2000) for (a) 1.5 °C and (b) 2.0 °C global warming time slices; and (c) the 2080–2099 period (under the RCP 8.5 scenario). Stippling indicates locations where the degree of change was statistically significant at the 95% confidence level.

under all warming scenarios considered (Fig. 1). Increases in the AT105F are also projected for eastern China, Southeast Asia, Australia, and the southeastern United States (Fig. 2). In these regions, relative humidity tends to decrease, but the elevated temperatures nevertheless cause increased heat stress. Compared with the changes under 1.5 °C warming, global warming at the 2.0 °C limit set by the Paris agreement results in a further rise in the frequency of danger heat conditions and expansion of affected areas. The total area affected under 2.0 °C warming is predicted to be about 15.6% larger than that under 1.5 °C warming. AT105F over the affected areas is 1.6 times and 2.3 times higher under 1.5 °C and 2.0 °C than under the current climate. Under the RCP 8.5 emissions scenario, even larger areas (79.3% of the total land area covered) – including regions at high latitudes – become subject to dangerous levels of heat stress by the end of the century (Fig. 2c). Moreover, the population in tropical regions will be subjected to dangerous heat conditions more frequently, since the HHI in these regions will exceed 105 °F for more than one third of the year.

We created an aggregate measure of each nation's overall exposure to extreme events by taking into consideration the degree of health heat stress, the area of land affected, and the relative size of the affected population (Fig. S3). If a country contains a grid cell with HHI > 105 °F for at least one day during the period of interest, the country is judged to be exposed to heat stress. The results for the baseline period (1981–2000) show that India and China experience the greatest threat from dangerously high levels of heat, owing to their high population intensity, followed by Brazil and several countries located in central Africa (Fig. 3). Future projections under 1.5 °C and 2.0 °C warming show that the number of countries exposed to heat stress will increase to 129 and 135 respectively, compared with the 109 heat-stressed countries in the baseline period. Newly affected regions will arise in the United States, Indonesia, and Australia. Developing countries are projected to remain the most vulnerable, with a higher exposure index and the least-developed infrastructure. About 26 and 54 countries will be subjected to more than double the HHI integrated heat stress exposure than that in the baseline period, under 1.5 °C and 2.0 °C warming, respectively. Current temperature and population trends are likely to impose significant additional health risks on low income, less developed countries. By the end of the 21st century, > 95% of countries will face exposure to health heat stress. The increase in HHI integrated exposure index will also affect highly developed nations, such as the United States, which is expected to be under threat from severe heat stress by 2100. India and Brazil rank highest for HHI integrated exposure, and will experience a more than doubling of heat-related health stress by the end of the 21st century, owing to increased severity of natural hazards and ongoing population growth (Fig. 3d).

3.2. Changes in wildfire risk

Wildfire is a vital component of terrestrial ecosystems, shaping the composition and functioning of terrestrial ecosystems and affecting the global carbon cycle. In recent years, increased occurrences of extremely destructive fires have been observed worldwide, triggering substantial socio-economic costs. Climate and weather, including temperature, humidity, precipitation, and wind speed, are the most important determinants of forest fire danger. We used the McArthur Forest Fire Danger Index, which unites these weather variables into a single metric, to measure the danger of fire and changes in the length of the fire season for diverse terrestrial ecosystems (Fig. S1, see Materials and methods section) under different global warming levels. Compared with the current climate state, the length of the fire season is expected to increase in the western United States, the Amazon Plain, northern China, Australia, and Central Asia under both 1.5 °C and 2.0 °C global warming targets (Fig. 4). The additional 0.5 °C warming between 1.5 °C and 2.0 °C appears to contribute mainly to increases in fire season length in the affected areas. The regional mean fire season length increases by 6.2 days and 9.5 days under 1.5 °C and 2.0 °C warmings, relative to the baseline period. Ecological model simulation further demonstrates that an increase in the frequency of wildfires is likely to occur in the western United States, Central Asia, and Australia under the 2.0 °C warming target, while there is no increase in fire frequency over large regions of the Amazon Plain. A comparison of the distribution of fire season length across the world's biomes under different warming states shows that tropical and subtropical forests, tropical and subtropical grasslands, Mediterranean forests, and desert biomes are more sensitive to climate fluctuations than other biomes, and exhibit increased threat from fires with global warming (Fig. 5). The median fire season length in these six biomes is projected to be longer than 50 days by the end of the 21st century. Large areas of forest are distributed as tropical and subtropical forest, and Mediterranean forest biome regions; therefore, increased fire season length with global warming may promote more frequent wildfires and bring about increases in tree mortality in these areas, with subsequent impact on the carbon cycle. Except for the tropical and subtropical grasslands, tundra, deserts and xeric shrublands, most biomes exhibit increases in fire frequency with global warming, as calculated by the Vegetation Integrative SImulator for Trace Gases (VISIT) model (see Methods). Biomes experiencing the greatest change in fire frequency are the tropical and subtropical coniferous forests and the Mediterranean forests (Fig. 5).

We calculated the relative magnitude of integrated exposure to wildfires at the country level by taking into consideration the biome area affected by wildfire and the frequency of wildfires. Over the baseline period, Australia and China have relatively greater exposure to wildfires than other countries (Fig. 6). The United States, Brazil, India, and Russia are other major countries threatened by wildfire. Under the 1.5 °C and 2.0 °C global warming targets, the exposure index in these countries increases, showing that wildfires are likely to worsen considerably in these countries. Moreover, almost all European countries

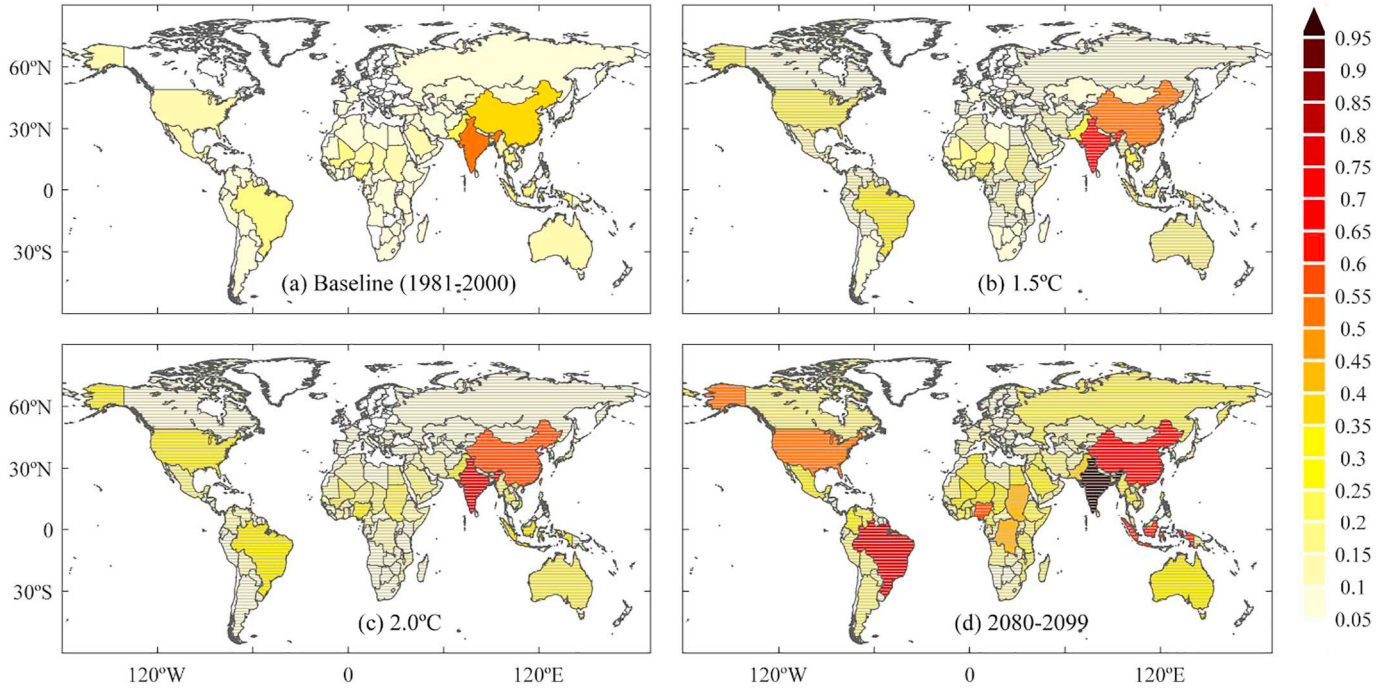

Fig. 3. Integrated exposure to dangerous heat stress during different global warming periods. Country-level average HHI-integrated exposure index values (dimensionless) for (a) the baseline period 1981–2000, (b) the 1.5 °C warming target, (c) the 2.0 °C warming target, and (d) the 2080–2099 RCP 8.5 period. Stippling in (b, c, d) indicates locations where the degree of change during different global warming periods, relative to the baseline period (a), was statistically significant at the 95% confidence level.

are predicted to face worsening fire risk with a 2.0 °C increase in global mean temperature. Under the RCP 8.5 scenario, fire risk substantially increases by the end of the 21st century over 74% of global land, in particular in the United States, Canada, Brazil, China, Australia, and Russia (Fig. 6d). The increase in the number of extremely destructive fires will pose a severe threat to ecological systems, possibly resulting in the extinction of tree species and disrupting the global biology cycle.

3.3. Changes in anthesis heat stress

Heat stress poses an important threat to agricultural production and global food security. Crops are especially vulnerable to high temperature episodes during their reproductive period. We calculated heat stress during the reproductive phase of development – anthesis heat stress (AHS) – to assess the potential damage to crop growth under

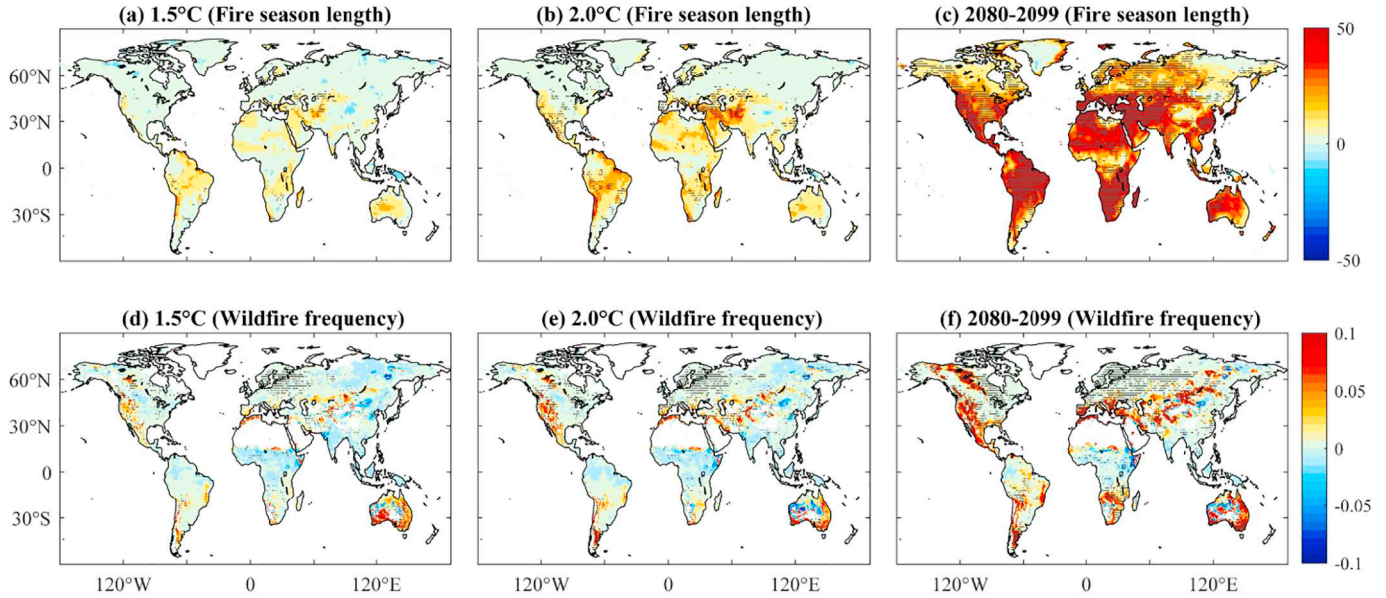

Fig. 4. Changes in fire season length and wildfire frequency. Changes in the average length of the fire season (days) under (a) 1.5 °C warming, (b) 2.0 °C warming, and (c) during the 2080–2099 period, relative to the baseline period 1981–2000. Changes in the frequency of wildfires under (d) 1.5 °C warming, (e) 2.0 °C warming, and (f) during the 2080–2099 period, relative to the baseline period 1981–2000. Stippling indicates locations where the degree of change was statistically significant at the 95% confidence level.

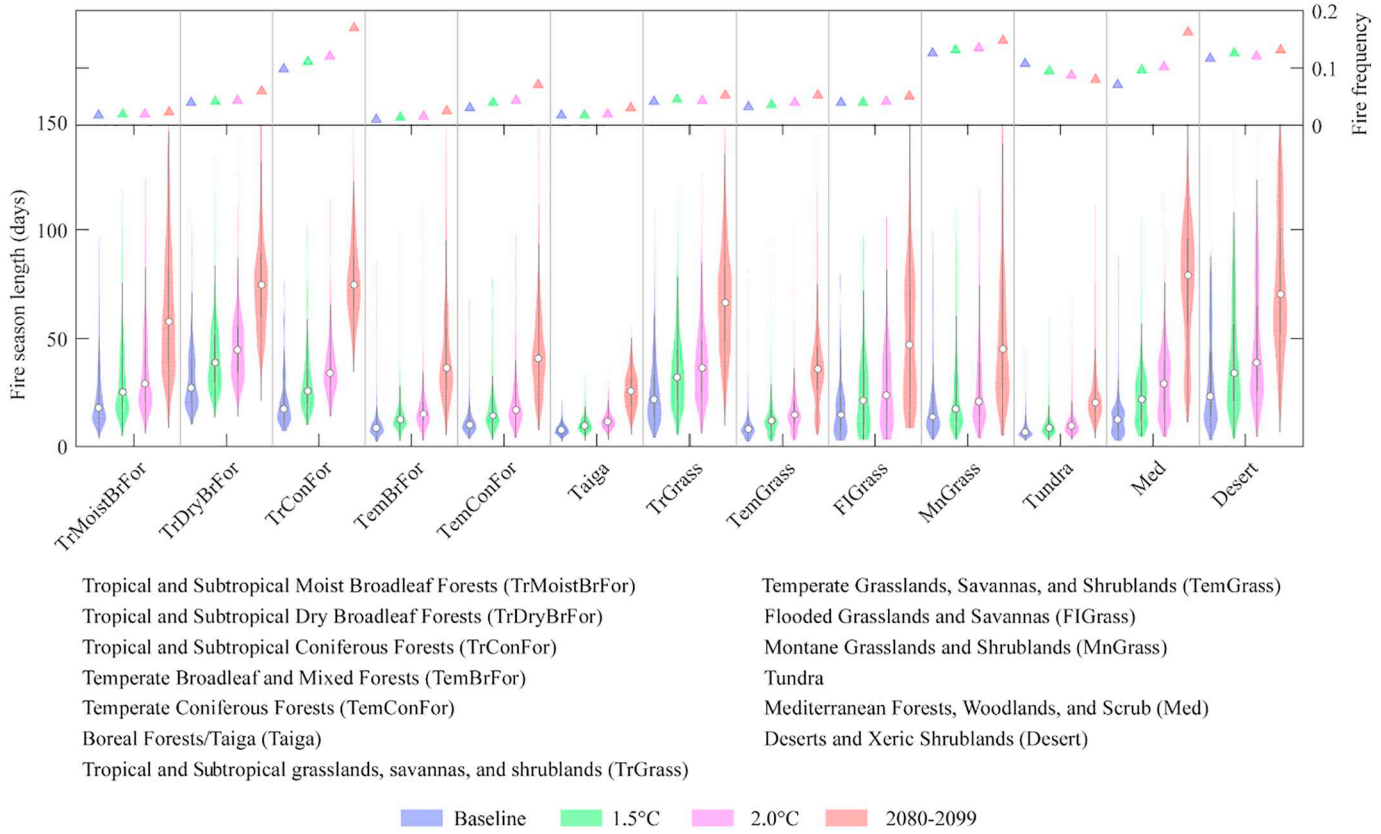

Fig. 5. Regional average fire frequency and distribution of fire-season length across the world's biomes. Fire frequency and fire-season length are shown for the baseline period 1981–2000 (blue), the 1.5 °C warming target (green), the 2.0 °C warming target (magenta), and the 2080–2099 period (red). Violin plots represent the probability distribution function for the fire season length in the different biomes. Circles indicate the median fire season length. (For interpretation of the references to color in this figure legend, the reader is referred to the web version of this article.)

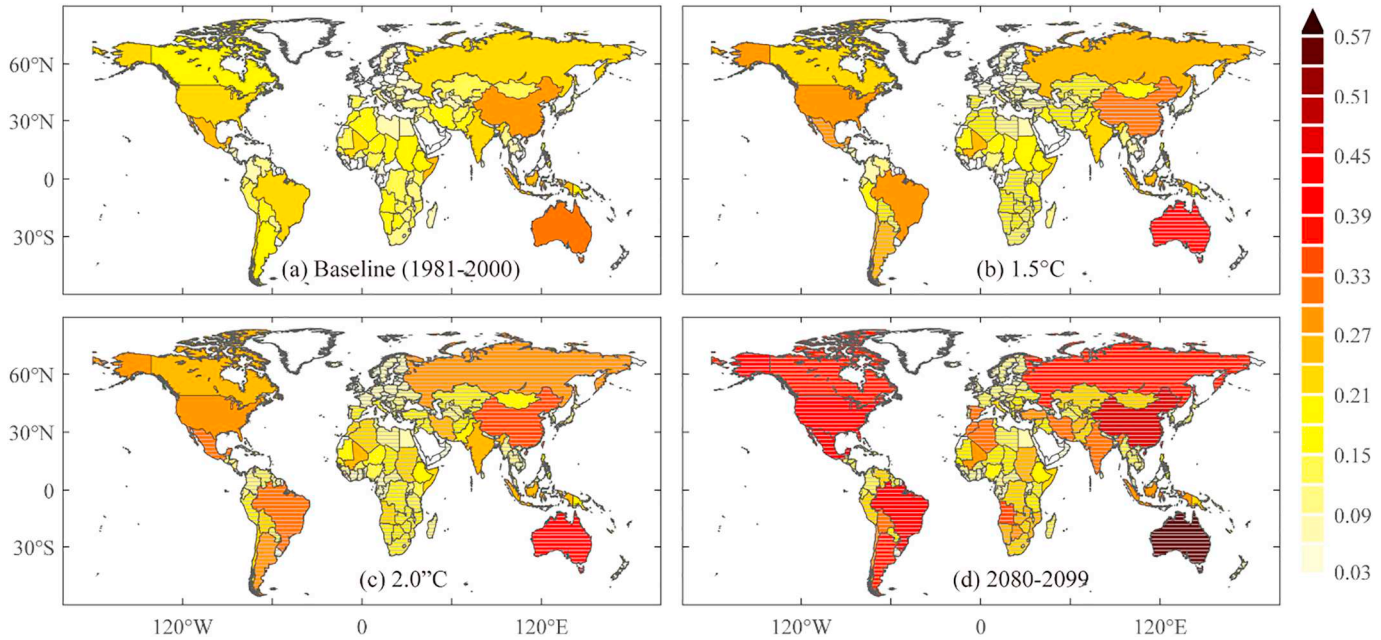

Fig. 6. Integrated exposure to wildfire during different global warming periods. Country-level wildfire exposure index for (a) the baseline period 1981–2000, (b) the 1.5 °C warming target, (c) the 2.0 °C warming target, and (d) the 2080–2099 RCP 8.5 period. Stippling in (b, c, d) indicates locations where the degree of change during different global warming periods, relative to the baseline period (a), was statistically significant at the 95% confidence level.

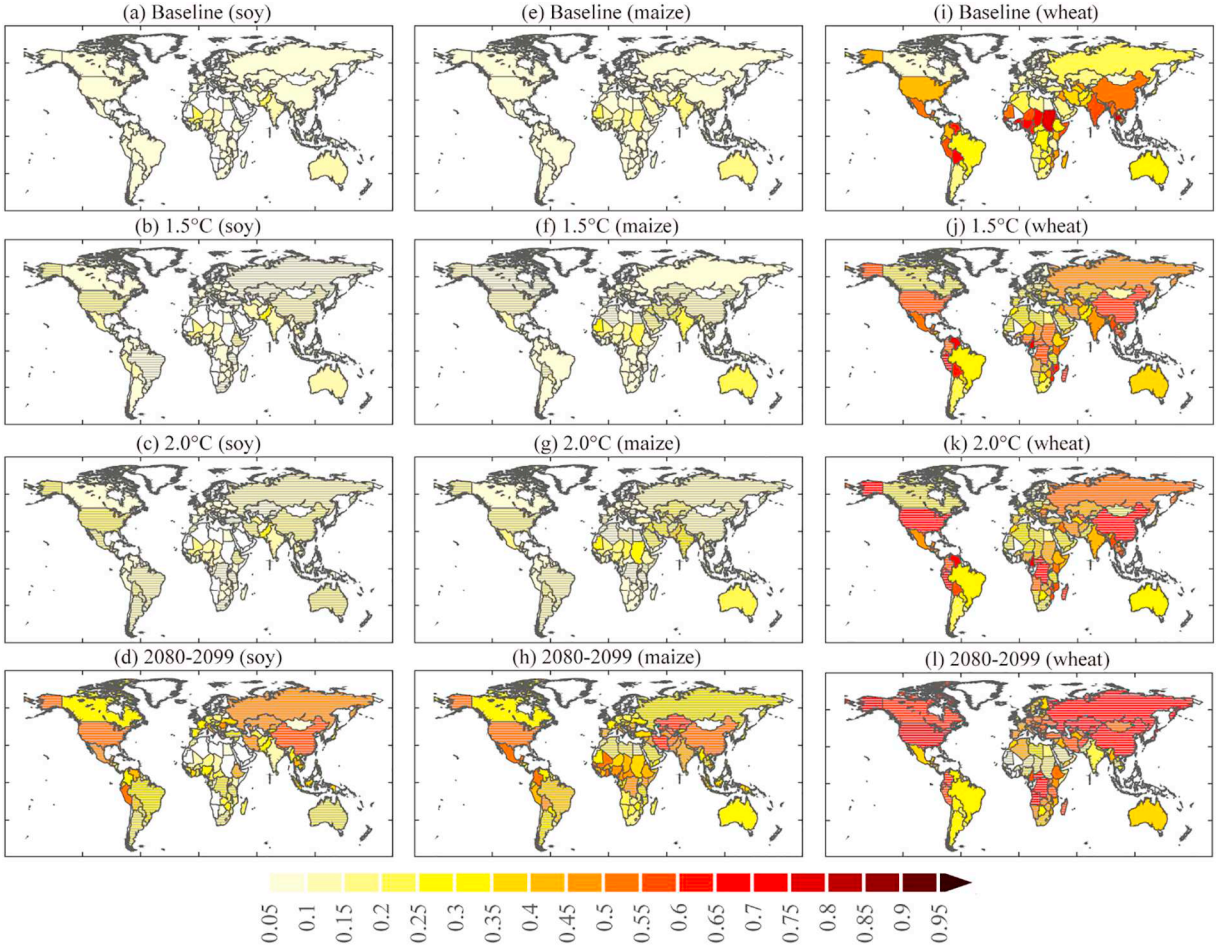

Fig. 7. Normalized agricultural production damage index during different global warming levels. Country-level normalized agricultural production damage index for (a) soybean, (e) maize, and (i) wheat during the baseline period (1981–2000); (b) soybean, (f) maize, and (j) wheat for the 1.5 °C global warming target; (c) soybean, (g) maize, and (k) wheat for the 2.0 °C global warming target; and (d) soybean, (h) maize, and (l) wheat for the 2080–2099 (RCP 8.5) period. Stippling in (b–d, f–h, j–l) indicates locations where the degree of change during different global warming periods, relative to the baseline period (a, e, i), was statistically significant at the 95% confidence level.

different levels of global warming. Wheat shows high AHS levels even in the baseline climate, particularly in South Asia, southern North America, sub-Saharan Africa, and southeastern China: 19.8%, 31.6%, 37.3%, and 69.3% of all grids suitable for wheat (Fig. S2) are affected by high or very high (AHS index > 0.15) stress intensity during the baseline period, 1.5 °C warming, 2.0 °C warming, and at the end of 21st century under RCP 8.5 (Fig. S4). Significant increases in AHS for wheat under 1.5 °C and 2.0 °C global warmings occur in the central United States, northwestern South Asia, and northern China. Areas with high AHS levels are projected to cover the Mediterranean region and extend into Central Asia under 2.0 °C global warming. By the end of the 21st century, almost all suitable cropping areas are likely to experience an increased number of high temperature episodes, resulting in very high AHS intensity. By contrast, maize, and soybean exhibit low AHS intensity in the baseline climate. Soybean and maize areas affected by high AHS intensity remain unaltered under 1.5 °C and 2.0 °C warmings, owing to their higher critical temperature thresholds (Table 2). With global warming, the main heat stress hot-spots for soybean and maize are predicted to occur in northwestern India and the southern United States, where AHS intensity is projected to increase to high or very high levels at certain grid locations. Consistent with the patterns of AHS shown in Fig. S4, Fig. 7 shows that crops in Iran, Pakistan, India, the United States, and countries in northern sub-Saharan Africa are more likely to be affected by high temperature episodes. In general, countries in tropical regions experience greater levels of exposure than other regions during the baseline period. With global warming, increasing numbers of countries become subject to more frequent, more severe high-temperature episodes, threatening agricultural production and food security.

Fig. S5 shows the projected changes in the production of soybean, maize, and wheat based on simulations by the PEGASU model, which predicts crop yields in response to heat stress. Under 1.5 °C global warming, the production of all crops is expected to decrease in tropical regions but increase in many high-latitude countries, especially Russia and European countries. Warmer, wetter climate states in high-latitude regions are conducive to crop development and result in more areas becoming suitable for agriculture, leading to increased production. In our study, we did not take CO_2-fertilization into consideration; the results obtained by Schleussner et al. (2016) suggested that the positive effects of CO_2-fertilization may counteract the negative effects of climate change, resulting in an overall increase in yields for soy and wheat and a slightly smaller reduction for maize under 1.5 °C and 2.0 °C warmings. Moreover, the increase in crop production at high latitudes under 1.5 °C warming (for example, wheat production in Russia and Mediterranean countries) may vanish at the end of the 21st century if climate warming is not limited. The regional average wheat production is predicted to decrease by 20% by the end of the 21st century, relative to the baseline period. More marked downward trends in crop production with increases in global warming can be seen in tropical countries, particularly in Africa, southern Asia, and South America,

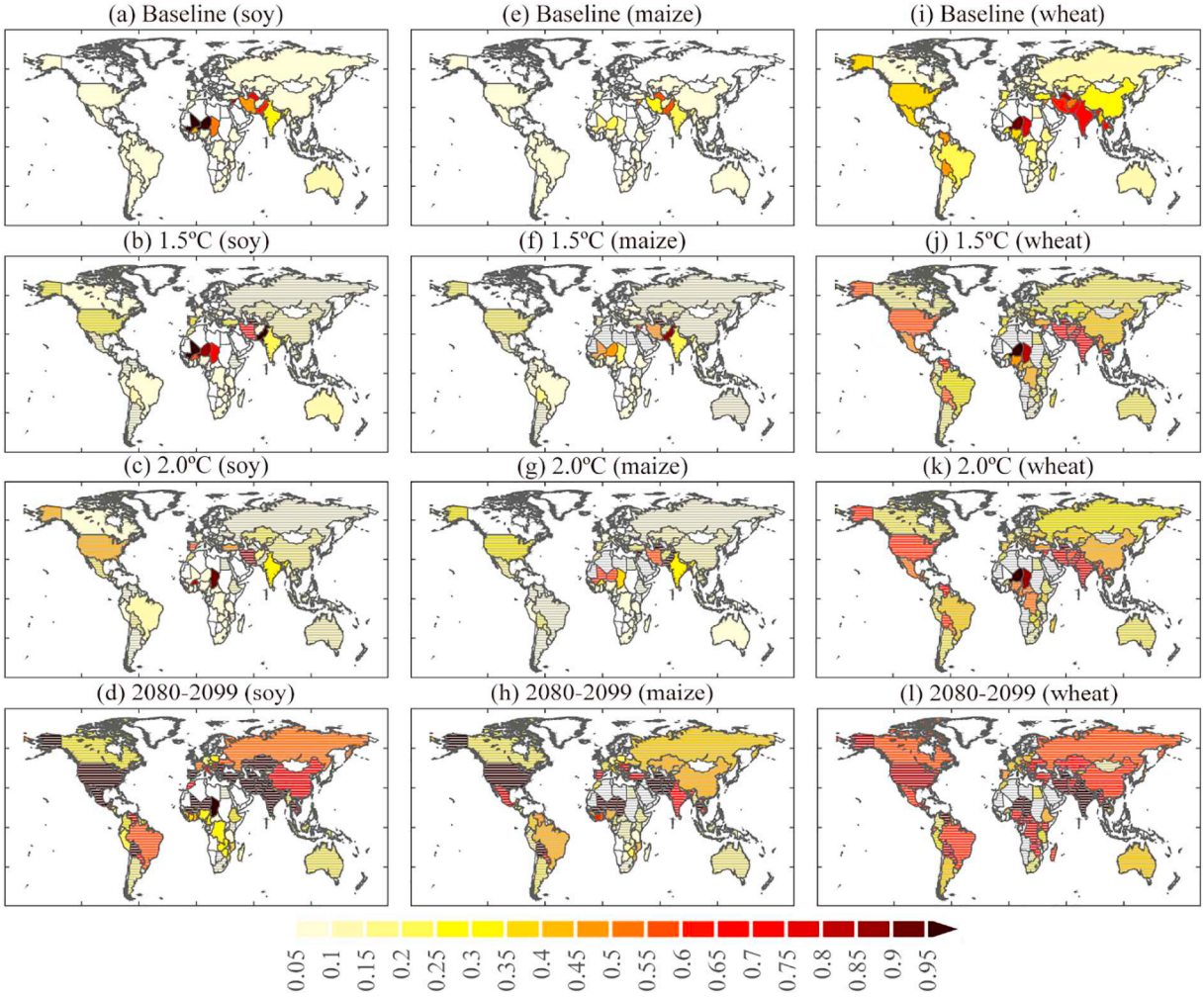

Fig. 8. Integrated exposure to crop heat stress during different global warming periods. Country-level crop-related exposure index for: (a) soybean, (e) maize, and (i) wheat during the baseline period (1981–2000); (b) soybean, (f) maize, and (j) wheat for the 1.5 °C global warming target; (c) soybean, (g) maize, and (k) wheat for the 2.0 °C global warming target; and (d) soybean, (h) maize, and (l) wheat for the 2080–2099 (RCP 8.5) period. Stippling in (b–d, f–h, j–l) indicates locations where the degree of change during different global warming periods, relative to the baseline period (a, e, i), was statistically significant at the 95% confidence level.

which are generally consistent with results presented by Challinor et al. (2014) and Asseng et al. (2015). At higher warming levels, the critical temperatures can be exceeded during the growing season, as shown in Fig. 7, resulting in diminished yields (Schauberger et al., 2017).

The normalized agricultural production damage index over the tropical regions is larger than that in other regions for all crops. Owing to the different critical temperatures for crops, soy and maize showed a lower normalized damage index with 1.5 °C and 2.0 °C warmings, but production of wheat suffered greater heat stress, with a higher normalized agricultural production damage index predicted for all climate scenarios. Decreased wheat production is predicted for 76, 90, and 115 countries under 1.5 °C warming, 2.0 °C warming, and in the 2080–2099 RCP 8.5 period. Increased normalized agricultural production damage index for wheat is projected for 106 countries. Under the RCP 8.5 scenario, almost all counties are predicted to suffer higher production damage and reductions in wheat production by the end of the 21st century, except Mongolia, Norway, and Sweden (Fig. S5, Fig. 7). It also should be noted that the normalized damage to soybean production is predicted to increase significantly by the end of the 21st century, especially in Russia, China, and the United States, driven mainly by the expansion of affected areas in these countries (Figs. 7, 8). Teixeira et al. (2013) also predict a large relative increase in agricultural production damage for soybean between the baseline period and the end of the 21st century. The relatively large increase in the effect of heat stress on soybean crops may be because only a small area is at risk under the baseline climate condition but, under future climate warming, there is a large increase in both the area affected by heat stress and the intensity of the heat stress.

3.4. Global warming of 2.0 °C: avoided impacts of the additional 0.5 °C increase in mean global temperature

Fig. 9 shows the proportion of impacts that are avoided under 1.5 °C warming as opposed to 2.0 °C warming. Globally, about 38%, 50%, 46%, 36%, and 48% of the increased exposure to health threats, wildfire, crop-related heat stress for soybeans, wheat, and maize could be avoided if global warming is to be restricted to 1.5 °C rather than 2 °C (based on the median values of the avoided impacts). In terms of exposure to health threats, constraining global warming to 1.5 °C instead of 2 °C would allow countries in tropical regions, including India and countries in Africa, to avoid many of the adverse effects of heat on health (Fig. 9a). Canada, Russia, Turkey, India, and countries in the Amazon basin and Mediterranean are relatively sensitive to the effects of climate warming on wildfires (Fig. 9b), which may have a significant impact on forests in these regions. Half a degree less warming (i.e. the 1.5 °C target) would help these countries avoid > 50% of the increased exposure to wildfire predicted to occur under 2 °C warming. Major food-producing countries, including the United States, China, and India,

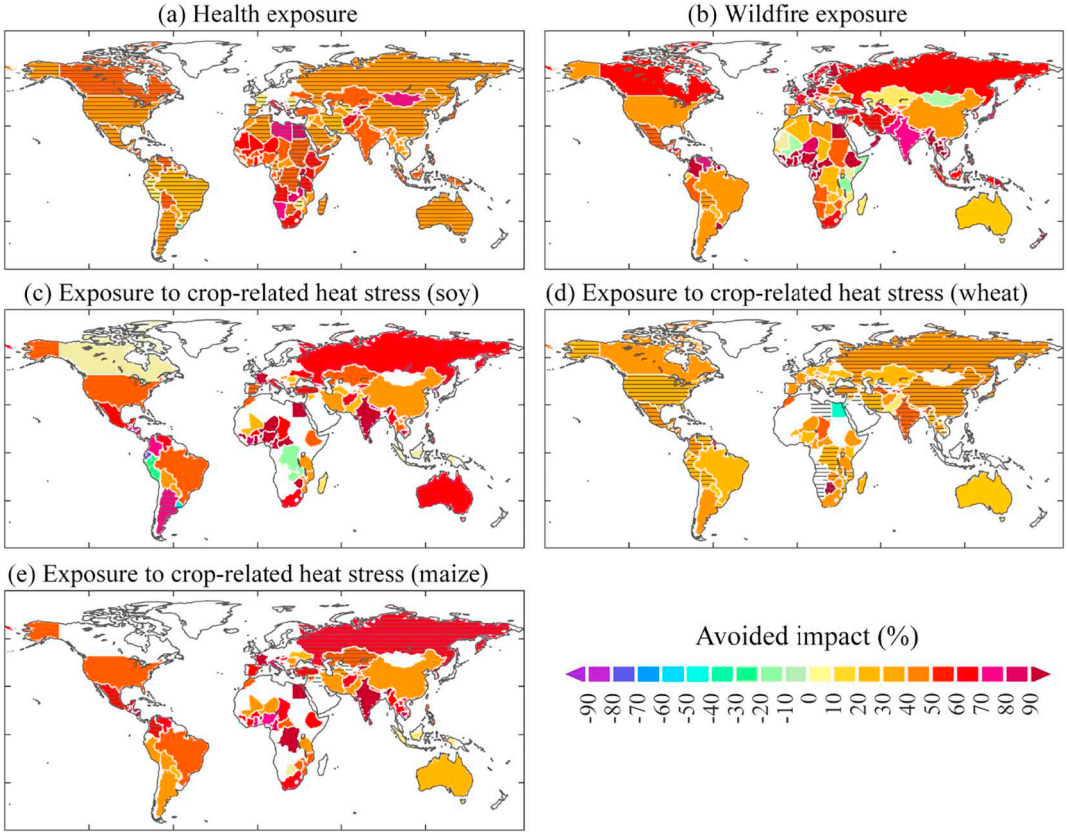

Fig. 9. Proportion of heat-related exposures avoided through 1.5 °C warming instead of 2 °C warming. (a) Health, (b) wildfire, (c) soybean, (d) wheat, and (e) maize sectors. Stippling indicates locations where the difference between the two levels was statistically significant at the 95% confidence level.

are vulnerable to enhanced crop heat stress associated with the additional 0.5 °C warming. With 2.0 °C global warming, food crises will continue to occur, and acute hunger is likely to intensify in certain food-deficient counties, such as in the Middle East and Africa. Larger impacts of heat stress are avoided for soybean and maize. It should be noted that there is a visual amplification of minor absolute changes for regions with low present-day exposure, in particular in the high northern latitudes.

4. Discussion and conclusions

We assessed changes in heat-related extremes for health, wildfire, and agricultural sectors under 1.5 °C and 2 °C global warmings. Relative magnitudes of climate and societal exposures were evaluated at the country level to identify hot-spot countries that respond the most to climate change. The results show that, even in a climate held to the 1.5 °C target, increases in the frequency and intensity of heat events should be expected. Under global warming, the increased daily temperature and associated changes to other weather variables will lead to more frequent, intense, and widespread heat-related extremes. First, heat-stress metrics that integrate the effects of rising humidity indicate that the risk of life-threatening heatwaves will increase (Im et al., 2017; Matthews et al., 2017). The additional 0.5 °C increase in mean global warming associated with the 2.0 °C target (compared with the 1.5 °C target) makes a significant difference to the extent of the area and the population exposure to extreme events. In a world with 1.5 °C global warming, 129 countries will be exposed to heat stress, and that number will rise to 135 with 2 °C global warming. Considering both the population and the areas exposed to heat stress, about 26 countries will be subjected to more than double the health-related heat integrated exposure under 1.5 °C global warming relative to the baseline period, and this increases to 54 countries under 2 °C warming. This will present a major challenge to developing countries, such as India, China, and Brazil. Over global land, about 38% of the increase health-related heat exposure can be avoided with 1.5 °C warming versus 2 °C warming.

In terms of the wildfire sector, previous studies have suggested that temporal inequality in the annual distribution of precipitation will increase in many regions with global warming, along with increases in the frequency of dry spells and dry days (Sillmann et al., 2013; Singh et al., 2014; Sun et al., 2018). The concurrence of hot, dry, and windy conditions is conducive to wildfires (Jolly et al., 2015). The fire danger index combines temperature, precipitation, and wind and confirms the lengthening of the fire season under global warming across almost all of the major vegetated regions in the world. Persistent lengthening of the fire season will likely lead to more frequent destruction of ecosystems by fire and an increase in the area burned, shortening the fire return intervals and threatening biodiversity. The additional 0.5 °C warming at 2.0 °C contributes mainly to increases in the duration of the fire season in the affected areas. The average length of the fire season over global land is projected to last 3.3 days longer with 2.0 °C warming than with 1.5 °C warming. A clear increase in the frequency of wildfires is projected to occur in the western United States, Canada, Mediterranean countries, Central Asia, and Australia under 2.0 °C warming; the biomes experiencing the greatest change in fire frequency are tropical and subtropical coniferous forests and Mediterranean forests. Previous studies (Moritz et al., 2012; Romero-Lankao et al., 2014) together with the IPCC Special Report on the impacts of global warming of 1.5 °C above pre-industrial levels (Hoegh-Guldberg et al., 2018) also indicate that the frequency of wildfires is projected to increase in over 37.8% of the global land area, with the risk of wildfire under 2 °C warming becoming particularly high in Canada, the United States, and Mediterranean countries. Globally, 0.5 °C less warming (i.e. the 1.5 °C target) would help avoid > 50% of the increased exposure to wildfire predicted to occur under 2 °C warming. By the end of the 21st century, the length of

the fire season and the frequency of wildfires are projected to increase substantially.

In terms of the agricultural sector, crops, particularly wheat, are likely to experience a greater number of high-temperature episodes during their reproductive period, posing a threat to crop production (Gao et al., 2014). The area suffering from high-intensity heat stress during the wheat reproductive phase is predicted to increase by 37.3% with 2.0 °C warming, covering the Mediterranean region and stretching into Central Asia. Moreover, the agricultural benefits of global warming in high-latitude regions may reduce or even disappear altogether with 2.0 °C warming. If specific climate-change mitigation targets and climate policies are not followed, and the RCP 8.5 emissions trajectory becomes reality, most regions of the world will be threatened by high-impact heat extremes by the end of the 21st century.

To identify hot-spot regions vulnerable to global warming, we compared the relative impact of heat-related extremes in the health, wildfire, and agricultural sectors across the world. It is not surprising that developing countries are likely to experience greater exposure to more serious heat extremes across multiple sectors than developed countries, a finding that is in agreement with recent studies. King and Harrington (2018) find that the poorest people would be subjected to the greatest changes in climate with a shift from 1.5 °C global warming to 2 °C global warming, and so propose greater support for climate adaptation to prevent poverty growth. Russo et al. (2019) suggest that exposure to heat hazards increases most in countries at lower levels of development, owing to larger increases in both the population growth and the risk of heatwave. Our predictions show that poorer countries are the most vulnerable, facing greater mortality, decreased food security, and increased forest fires, owing to their large populations and insufficient economic carrying capacity to resist the high risks associated with climate extremes. For instance, India is a large agricultural country with high population density and rich forests; it exports agricultural products to many nations. Our findings indicate that India will suffer multiple negative effects from climate change, including an increase in heat-related mortality, a marked decline in agricultural production, and an increased risk of forest fires, which not only threatens India's own security and income (Carleton, 2017) but also potentially affects food security and the carbon cycle across the world. Moreover, it should be noted that certain developed countries will also be affected adversely by severe heat stress under constantly rising temperatures: for example, health-related heat exposure in the United States and the risk of forest fires in Russia both increase under 2.0 °C global warming. Thus, according to both the avoided impacts index and previous studies that took different pathways for future societal development into account (King and Harrington, 2018; Russo et al., 2019), although the degree of response to global warming differs in different regions, both developing and developed countries will benefit greatly if global warming is stabilized below 1.5 °C.

It should be noted that our assessment of the changes in heat-related extremes at different levels of global warming is mainly based on climate model simulations, assisted by global impact models. Although uncertainty is associated with the projections, this study finds a consistent increase in risk with global warming, and so supports appeals for immediate mitigation measures to be implemented. International variations in the threat posed by climate change require that measurement indices account for the potential heterogeneity in socio-climatic factors.

Data availability

All data supporting the findings of this study are freely available from the following locations:

ISI-MIP Fast Track database: https://esg.pik-potsdam.de/search/isimip-ft.

Global dataset of gridded population scenarios: http://www.cger.nies.go.jp/gcp/population-and-gdp.html.

Terrestrial Ecoregions of the World: https://www.worldwildlife.org/publications/terrestrial-ecoregions-of-the-world

Global Harvested Area and Yield for 175 Crops dataset: http://www.earthstat.org/data-download/.

Acknowledgments

Funding for this research was provided by the National Natural Science Foundation of China (No. 41622101; No. 41877155), the State Key Laboratory of Earth Surface Processes and Resource Ecology, and the Fundamental Research Funds for the Central Universities. We acknowledge the modelling groups that participated in the Inter Sectoral Impact Model Intercomparison Project (ISI-MIP) for producing and making available their model output.

Appendix A. Supplementary data

Supplementary data to this article can be found online at https://doi.org/10.1016/j.envint.2019.04.025.

References

AghaKouchak, A., Cheng, L., Mazdiyasni, O., Farahmand, A., 2014. Global warming and changes in risk of concurrent climate extremes: insights from the 2014 California drought. Geophys. Res. Lett. 41, 8847–8852. https://doi.org/10.1002/2014GL062308.

AghaKouchak, A., Feldman, D., Hoerling, M., Huxman, T., Lund, J., 2015. Recognize anthropogenic drought. Nature 524, 409–4011. https://doi.org/10.1038/524409a.

Ahmadalipour, A., Moradkhani, H., 2018. Escalating heat-stress mortality risk due to global warming in the Middle East and North Africa (MENA). Environ. Int. 117, 215–225. https://doi.org/10.1016/j.envint.2018.05.014.

Ahmadalipour Moradkhani, H., Demirel, M., 2017. A comparative assessment of projected meteorological and hydrological droughts: elucidating the role of temperature. J. Hydrol. 553, 785–797. https://doi.org/10.1016/j.jhydrol.2017.08.047.

Asseng, S., et al., 2015. Rising temperatures reduce global wheat production. Nat. Clim. Change 5, 143–147. https://doi.org/10.1038/Nclimate2470.

Baker, H.S., Millar, R.J., Karoly, D.J., Beyerle, U., Guillod, B.P., Mitchell, D., Shiogama, H., Sparrow, S., Woollings, T., Allen, M.R., 2018. Higher CO_2 concentrations increase extreme event risk in a 1.5 °C world. Nat. Clim. Change 8, 604–608. https://doi.org/10.1038/s41558-018-0190-1.

Cai, W.J., Wang, G.J., Gan, B.L., Wu, L.X., Santoso, A., Lin, X.P., 2018. Stabilised frequency of extreme positive Indian Ocean dipole under 1.5 °C warming target. Nat. Commun. 9, 1–8. https://doi.org/10.1038/s41467-018-03789-6.

Carleton, T.A., 2017. Crop-damaging temperatures increase suicide rates in India. Proc. Natl. Acad. Sci. U. S. A. 114, 8746–8751. https://doi.org/10.1073/pnas.1701354114.

Challinor, A.J., Watson, J., Lobell, D.B., Howden, S.M., Smith, D.R., Chhetri, N., 2014. A meta-analysis of crop yield under climate change and adaptation. Nat. Clim. Change 4, 287–291. https://doi.org/10.1038/Nclimate2153.

Deryng, D., Conway, D., Ramankutty, N., Price, J., Warren, R., 2014. Global crop yield response to extreme heat stress under multiple climate change futures. Environ. Res. Lett. 9, 034011. https://doi.org/10.1088/1748-9326/9/3/034011.

Diffenbaugh, N.S., Giorgi, F., Raymond, L., Bi, X.Q., 2007. Indicators of 21st century socioclimatic exposure. Proc. Natl. Acad. Sci. U. S. A. 104, 20195–20198. https://doi.org/10.1073/pnas.0706680105.

Fischer, E.M., Knutti, R., 2015. Anthropogenic contribution to global occurrence of heavy-precipitation and high-temperature extremes. Nat. Clim. Change 5, 560–564. https://doi.org/10.1038/nclimate2617.

Fischer, E.M., Schar, C., 2010. Consistent geographical patterns of changes in high-impact European heatwaves. Nat. Geosci. 3, 398–403. https://doi.org/10.1038/ngeo866.

Fricko, O., et al., 2017. The marker quantification of the Shared Socioeconomic Pathway 2: A middle-of-the-road scenario for the 21st century. Glob. Environ. Chang. 42, 251–267. https://doi.org/10.1016/j.gloenvcha.2016.06.004.

Frieler, K., Meinshausen, M., Golly, A., Mengel, M., Lebek, K., Donner, S.D., Hoegh-Guldberg, O., 2013. Limiting global warming to 2 degrees C is unlikely to save most coral reefs. Nat. Clim. Change 3, 165–170. https://doi.org/10.1038/nclimate1674.

Gao, Y., Zhu, X.J., Yu, G.R., He, N.P., Wang, Q.F., Tian, J., 2014. Water use efficiency threshold for terrestrial ecosystem carbon sequestration under afforestation in China. Agric. For. Meteorol. 195-196, 32–37. https://doi.org/10.1016/j.agrormet.2014.04.010.

Gao, Y., Jia, Y.L., Yu, G.R., He, N.P., Zhang, L., Zhu, B., Wang, Y.F., 2019. Anthropogenic reactive nitrogen deposition and associated nutrient limitation effect on gross primary productivity in inland water of China. J. Clean. Prod. 208, 530–540. https://doi.org/10.1016/j.jclepro.2018.10.137.

Hempel, S., Frieler, K., Warszawski, L., Schewe, J., Piontek, F., 2013. A trend-preserving bias correction - the ISI-MIP approach. Earth Syst. Dynam. 4, 219–236. https://doi.org/10.5194/esd-4-219-2013.

Hoegh-Guldberg, O., et al., 2018: Impacts of 1.5°C global warming on natural and human systems. In: Global Warming of 1.5 °C. an IPCC Special Report on the Impacts of Global Warming of 1.5 °C above Pre-Industrial Levels and Related Global Greenhouse

Gas Emission Pathways, in the Context of Strengthening the Global Response to the Threat of Climate Change, Sustainable Development, and Efforts to Eradicate Poverty [Masson-Delmotte, V., P. Zhai, H.-O. Pörtner, D. Roberts, J. Skea, P.R. Shukla, A. Pirani, W. Moufouma Okia, C. Péan, R. Pidcock, S. Connors, J.B.R. Matthews, Y. Chen, X. Zhou, M.I. Gomis, E. Lonnoy, T. Maycock, M.Tignor, and T. Waterfeld (eds.)]. (In Press).

Huang, J.P., Yu, H.P., Dai, A.G., Wei, Y., Kang, L.T., 2017. Drylands face potential threat under 2 degrees C global warming target. Nat. Clim. Change 7, 417–422. https://doi.org/10.1038/nclimate3275.

Im, E.S., Pal, J.S., Eltahir, E.A., 2017. Deadly heat waves projected in the densely populated agricultural regions of South Asia. Sci. Adv. 3, e1603322. https://doi.org/10.1126/sciadv.1603322.

Jia, J.J., Gao, Y., 2017. Acid deposition and assessment of its critical load for the environmental health of waterbodies in a subtropical watershed, China. J. Hydrol. 555, 155–168. https://doi.org/10.1016/j.jhydrol.2017.10.017.

Jolly, W.M., Cochrane, M.A., Freeborn, P.H., Holden, Z.A., Brown, T.J., Williamson, G.J., Bowman, D.M.J.S., 2015. Climate-induced variations in global wildfire danger from 1979 to 2013. Nat. Commun. 6, 1–11. https://doi.org/10.1038/ncomms8537.

Keetch, J.J., Byram, G.M., 1968. A Drought Index for Forest Fire Control. Res. Pap. SE-38. vol. 38 US Department of Agriculture, Forest Service, Southeastern Forest Experiment Station, Asheville, NC 35 p.

Kharin, V.V., Flato, G.M., Zhang, X., Gillett, N.P., Zwiers, F., Anderson, K.J., 2018. Risks from climate extremes change differently from 1.5 °C to 2.0 °C depending on rarity. Earth's Future 6, 704–715. https://doi.org/10.1002/2018EF000813.

King, A.D., Harrington, L.J., 2018. The inequality of climate change from 1.5 to 2 °C of global warming. Geophys. Res. Lett. 45, 5030–5033. https://doi.org/10.1029/2018GL078430.

King, A.D., Karoly, D., 2017. Climate extremes in Europe at 1.5 and 2 °C of global warming. Environ. Res. Lett. 12, 114031. https://orcid.org/0000-0001-9006-5745.

King, A.D., Karoly, D.J., Henley, B.J., 2017. Australian climate extremes at 1.5 °C and 2 °C of global warming. Nat. Clim. Change 7, 412–416. https://doi.org/10.1038/nclimate3296.

Lehner, F., Coats, S., Stocker, T.F., Pendergrass, A.G., Sanderson, B.M., Raible, C.C., Smerdon, J.E., 2017. Projected drought risk in 1.5 °C and 2 °C warmer climates. Geophys. Res. Lett. 44, 7419–7428. https://doi.org/10.1002/2017GL074117.

Li, D.H., Zhou, T.J., Zou, L.W., Zhang, W.X., Zhang, L.X., 2018a. Extreme high-temperature events over East Asia in 1.5 degrees C and 2 degrees C warmer futures: analysis of NCAR CESM low-warming experiments. Geophys. Res. Lett. 45, 1541–1550. https://doi.org/10.1002/2017GL076753.

Li, D.H., Zou, L.W., Zhou, T.J., 2018b. Extreme climate event changes in China in the 1.5 and 2 degrees C warmer climates: results from statistical and dynamical downscaling. J. Geophys. Res.-Atmos. 123, 10196–10211. https://doi.org/10.1029/2018JD028835.

Lung, T., Lavalle, C., Hiederer, R., Dosio, A., Bouwer, L.M., 2013. A multi-hazard regional level impact assessment for Europe combining indicators of climatic and non-climatic change. Glob. Environ. Chang. 23, 522–536. https://doi.org/10.1016/j.gloenvcha.2012.11.009.

Matthews, T.K., Wilby, R.L., Murphy, C., 2017. Communicating the deadly consequences of global warming for human heat stress. Proc. Natl. Acad. Sci. U. S. A. 114, 3861–3866. https://doi.org/10.1073/pnas.1617526114.

Monfreda, C., Ramankutty, N., Foley, J.A., 2008. Farming the planet: 2. Geographic distribution of crop areas, yields, physiological types, and net primary production in the year 2000. Glob. Biogeochem. Cycles 22, GB1022. https://doi.org/10.1029/2007GB002947.

Moritz, M.A., Parisien, M.A., Batllori, E., Krawchuk, M.A., Van Dorn, J., Ganz, D.J., Hayhoe, K., 2012. Climate change and disruptions to global fire activity. Ecosphere 3, 1–22. https://doi.org/10.1890/ES11-00345.1.

Murakami, D., Yamagata, Y., 2016. Estimation of gridded population and GDP scenarios with spatially explicit statistical downscaling. ArXiv, 1610.09041, URL: https://arxiv.org/abs/1610.0904.

Nangombe, S., Zhou, T.J., Zhang, W.X., Wu, B., Hu, S., Zou, L.W., Li, D.H., 2018. Record-breaking climate extremes in Africa under stabilized 1.5 degrees C and 2 degrees C global warming scenarios. Nat. Clim. Change 8, 375–+. https://doi.org/10.1038/s41558-018-0145-6.

NOAA, 1985. Heat Wave: A Major Summer Killer. NOAA/PA 850001, NOAA/NCDC, Asheville, NC.

Noble, I.R., Bary, G.A.V., Gill, A.M., 1980. Mcarthur fire-danger meters expressed as equations. Aust. J. Ecol. 5, 201–203. https://doi.org/10.1111/j.1442-9993.1980.tb01243.x.

Olson, D.M., et al., 2001. Terrestrial ecoregions of the world: a new map of life on Earth. Bioscience 51, 933–938. https://doi.org/10.1641/0006-3568(2001)051[0933:TEOTWA]2.0.CO;2.

Romero-Lankao, P. et al., 2014: North America. In: Climate Change 2014: Impacts, Adaptation, and Vulnerability. Part B: Regional Aspects. Contribution of Working Group II to the Fifth Assessment Report of the Intergovernmental Panel on Climate Change [Barros, V.R., C.B. Field, D.J. Dokken, M.D. Mastrandrea, K.J.

Rosenzweig, C., et al., 2014. Assessing agricultural risks of climate change in the 21st century in a global gridded crop model intercomparison. Proc. Natl. Acad. Sci. U. S. A. 111, 268–3273. https://doi.org/10.1073/pnas.1222463110.

Rothfusz, L.P., 1990. The heat index equation. In: National Weather Service Technical Attachment (SR 90–23).

Russo, S., Sillmann, J., Sippel, S., Barcikowska, M.J., Ghisetti, C., Smid, M., O'Neill, B., 2019. Half a degree and rapid socioeconomic development matter for heatwave risk. Nat. Commun. 10. https://doi.org/10.1038/s41467-018-08070-4.

Schauberger, B., et al., 2017. Consistent negative response of US crops to high temperatures in observations and crop models. Nat. Commun. 8. https://doi.org/10.1038/ncomms13931.

Schleussner, C.F., et al., 2016. Differential climate impacts for policy-relevant limits to global warming: the case of 1.5 °C and 2 °C. Earth Syst. Dynam 7, 327–351. https://doi.org/10.5194/esd-7-327-2016.

Sillmann, J., Kharin, V.V., Zwiers, F.W., Zhang, X., Bronaugh, D., 2013. Climate extremes indices in the CMIP5 multimodel ensemble: part 2. Future climate projections. J. Geophys. Res. - Atmos. 118, 2473–2493. https://doi.org/10.1002/jgrd.50188.

Singh, D., Tsiang, M., Rajaratnam, B., Diffenbaugh, N.S., 2014. Observed changes in extreme wet and dry spells during the South Asian summer monsoon season. Nat. Clim. Change 4, 456–461. https://doi.org/10.1038/nclimate2208.

Sun, Q., Miao, C., AghaKouchak, A., Duan, Q., 2017. Unraveling anthropogenic influence on the changing risk of heat waves in China. Geophys. Res. Lett. 44, 5078–5085. https://doi.org/10.1002/2017GL073531.

Sun, Q., Miao, C., Duan, Q., Ashouri, H., Sorooshian, S., Hsu, K., 2018. A review of global precipitation data sets: data sources, estimation, and intercomparisons. Rev. Geophys. 56, 79–107. https://doi.org/10.1002/2017RG000574.

Teixeira, E.I., Fischer, G., van Velthuizen, H., Walter, C., Ewert, F., 2013. Global hot-spots of heat stress on agricultural crops due to climate change. Agric. For. Meteorol. 170, 206–215. https://doi.org/10.1016/j.agrformet.2011.09.002.

Wang, Z.L., Lin, L., Zhang, X.Y., Zhang, H., Liu, L.K., Xu, Y.Y., 2017. Scenario dependence of future changes in climate extremes under 1.5 degrees C and 2 degrees C global warming. Sci. Rep. 7. https://doi.org/10.1038/Srep46432.

Williams, A.P., et al., 2013. Temperature as a potent driver of regional forest drought stress and tree mortality. Nat. Clim. Chang. 3, 292–297. https://doi.org/10.1038/nclimate1693.

Xu, Y., et al., 2017. Asian climate change under 1.5–4 °C warming targets. Adv. Clim. Change Res. 8, 99–107. https://doi.org/10.1016/j.accre.2017.05.004.

Yang, Y., Jia, X., Wendroth, O., Liu, B., Shi, Y., Huang, T., Bai, X., 2019. Noise-assisted multivariate empirical mode decomposition of saturated hydraulic conductivity along a south-north transect across the Loess Plateau of China. Soil Sci. Soc. Am. J. https://doi.org/10.2136/sssaj2018.11.0438.

Zhang, W.X., Zhou, T.J., Zou, L.W., Zhang, L.X., Chen, X.L., 2018. Reduced exposure to extreme precipitation from 0.5 degrees C less warming in global land monsoon regions. Nat. Commun. 9. https://doi.org/10.1038/S41467-018-05633-3.

Zhou, T., Ren, L., Liu, H., Lu, J., 2018. Impact of 1.5 °C and 2.0 °C global warming on aircraft takeoff performance in China. Sci. Bull. 63, 700–707. https://doi.org/10.1016/j.scib.2018.03.018.

Zhou, T., et al., 2018a. When and how will the millennium silk road witness 1.5 °C and 2 °C warmer worlds? Atmos. Oceanic Sci. Lett. 11, 180–188. https://doi.org/10.1080/16742834.2018.1440134.